Electrical Power and Energy Systems 157 (2024) 109828

Contents lists available at ScienceDirect

International Journal of Electrical Power and Energy Systems

journal homepage: www.elsevier.com/locate/ijepes

Sequential power flow algorithm and post-event steady-state power distribution analysis in hybrid AC/MT-MVDC systems

Pingyang Sun [a,*], Rongcheng Wu [b], Zhiwei Shen [a], Gen Li [c], Muhammad Khalid [d], Graham Town [e], Georgios Konstantinou [a]

[a] School of Electrical Engineering and Telecommunications, UNSW Sydney, Sydney, NSW, 2052, Australia
[b] Data Science Institute, University of Technology Sydney, NSW, 2007, Australia
[c] Department of Engineering Technology and Didactics Electric Energy, Technical University of Denmark, Ballerup, 2750, Denmark
[d] Electrical Engineering Department & Interdisciplinary Research Center for Renewable Energy and Power Systems, King Fahd University of Petroleum & Minerals, Dhahran, 31261, Saudi Arabia
[e] School of Engineering, Macquarie University, NSW, 2109, Australia

ARTICLE INFO

Keywords:
Hybrid AC/MT-MVDC system
MVDC distribution network
Voltage source converter (VSC)
Dc/dc converter
Power flow (PF)
Power distribution
Droop control

ABSTRACT

In hybrid ac/multi-terminal medium-voltage dc (AC/MT-MVDC) systems with multiple voltage source converters (VSCs) and dc/dc converters, it is essential to attain accurate initial power flow (PF) and post-event power distribution solutions efficiently. This paper proposes: (i) a novel sequential PF algorithm for hybrid AC/MT-MVDC systems by a Fibonacci search-based Newton–Raphson (FSNR) approach with uniform MVDC bus type definition, while considering power losses and varied control schemes of different converters; (ii) a zero error steady-state post-event power distribution calculation method under droop control by the introduction of dynamic I/V droop coefficients based on the FS algorithm. The FSNR approach simplifies the MVDC PF derivation by only requiring the definition of the dc current bus type, effectively eliminating the need to solve multiple sub-Jacobian matrices. Furthermore, the post-event power distribution analysis offers precise power redistribution calculation approach following disturbances by considering both open- and closed-loop operation in an MT-MVDC distribution system. The computational efficiency and validity of the proposed PF algorithm, along with the accuracy of presented post-event power distribution calculation method are verified through Python and RTDS real-time simulators in an extended MT-MVDC distribution network incorporated with the IEEE 14/33/69 bus transmission/distribution systems.

1. Introduction

Medium-voltage dc (MVDC) systems within distribution grids facilitate the integration of dc devices while simultaneously enhancing the power supply quality, reliability, and stability [1]. Voltage source converters (VSCs) are the predominant ac/dc (dc/ac) converters, due to the flexible power control ability and possible power delivery capability under weak grids [2]. Dc/dc converters are also prevalently found in MVDC systems for MV/LV level change [3]. Many network configurations are available in MVDC distribution systems, including radial, ring and meshed structures with multiple VSCs and dc/dc converters [1]. The VSC and dc/dc converter-connected MVDC terminals can be interconnected in a variety of manners, forming multi-terminal MVDC (MT-MVDC) systems [4–6].

To ensure static operational security and enhance system planning/design for future MVDC networks, it is essential to investigate the detailed power distribution within the MVDC network. This includes (1) the initial power flow (PF), and (2) the post-event power distribution after acquiring the initial operational conditions. The PF for ac distribution systems can be determined by backward/forward sweep (BFS) [7], improved Newton–Raphson (NR) approaches [8], etc. The conventional NR method is not suitable for radial MVAC distribution systems due to the large ratio between the resistance and reactance (R/X) in feeders. However, it can still be applied in the MVDC PF determination of MT-MVDC systems since only line resistance is considered.

In an MT-MVDC distribution system, multiple VSCs and dc/dc converters are directly interlinked by different MVDC terminals. Therefore, it is necessary to include the impact of power losses and diverse control strategies of VSCs and dc/dc converters on the overall PF computation for MVDC distribution systems. Current studies on PF for dc microgrids

* Corresponding author.
E-mail address: pingyang.sun@student.unsw.edu.au (P. Sun).

https://doi.org/10.1016/j.ijepes.2024.109828
Received 23 September 2023; Received in revised form 29 November 2023; Accepted 18 January 2024
Available online 28 January 2024

Nomenclature

$\mathcal{A}$	Current deviation coefficient after closing tie switches
$\mathcal{B}$	Current deviation coefficient after disconnecting lines
ΔI_{dcm}^{cor}	DC current deviation
$\Delta K_{droop}^{IV,pv}$	I/V droop coefficient deviation
δ_{droop}	Maximum allowable dc voltage diviation ratio
$K_{droop}^{IV,pv}$	Dynamic I/V droop coefficient
$\mathcal{L}_{\Delta}$	Left searching margin
$\mathcal{M}_{\Delta}$	Middle value in each searching step
$\mathcal{R}_{\Delta}$	Right searching margin
C_c	Loss coefficients in VSCs
G_{dcm}	Line conductance
I_c	AC current in VSCs
I_{dcm}	DC current at the LVDC link
I_{dcm}	DC current at the MVDC link
I_{dcm}^{act}	Actual DC current
I_{dcm}^{est}	Estimated DC current
I_{dcrefm}	DC current reference
I_{line}	line current in MVDC systems
I_{tie}	Tie switch current in MVDC systems
J_{dcm}	Jacobian matrix
K_{droop}	Droop coefficient
$K_{droop}^{IV est,pv}$	Estimated I/V Droop coefficient
$K_{droop}^{IV vir,pv}$	Virtual I/V Droop coefficient
P_c	AC active power at the converter side of VSCs
P_{dcl}	DC power at the LVDC link
P_{dcm}	DC power at the MVDC link
P_{dcm}^{pre}	Pre-specified DC power
P_{dcm}^{tar}	Target DC power
P_{dcrefm}	DC power reference
P_d	AC active power at MVAC bus
P_{ge}	AC active power of generators at HVAC bus
$P_{loss,c}$	Power losses in VSCs
P_{lossm}	Power losses in DC/DC converters
P_{lo}	AC active power of connected loads
P_s	AC active power at the grid side of VSCs
P_s'	AC active power from the MVAC system
Q_c	AC reactive power at the converter side of VSCs
Q_d	AC reactive power at MVAC bus
Q_{ge}	AC reactive power of generators at HVAC bus
Q_{lo}	AC reactive power of connected loads
Q_s	AC reactive power at the grid side of VSCs
Q_s'	AC reactive power from the MVAC system
R_e	Equivalent resistance of AC transformer
R_{lossm}	Equivalent resistance in DC/DC converters
$V_{dcm,rated}$	Rated MVDC voltage
V_{dcm}	DC voltage at the MVDC link
V_{dcrefm}	DC voltage reference
X_e	Equivalent reactance of AC transformer
Y_{br}	Branch admittance matrix in the MVAC system

address convex approximation for optimal PF [9,10], explore the droop characteristics of distributed generators (DGs) during both normal [11, 12] and island operations [13], and delve into the maximum power point tracker (MPPT) control for DGs [14]. However, there is limited analysis on the converter impact on PF. In HVDC transmission systems, only the VSCs are included in PF studies, either for sequential [15–17] or unified algorithms solving ac and dc PFs [18,19]. In addition, various types of dc buses are predefined for the computation in conventional dc PF analysis of HVDC systems [17] and dc microgrids [11]. These types include power buses, current buses, and voltage droop buses, with the exception of the dc slack bus. The need to establish and solve multiple sub-Jacobian matrices complicates the bus type definition process. A simplified bus type definition is necessary for dc PF analysis, considering the significant number of converters featuring diverse control modes in MT-MVDC distribution systems.

The post-event power distribution, for example after a station or line failure, is also critical for static security assessment of MT-MVDC systems [20]. Detailed power redistribution analysis for VSC-based HVDC transmission systems after different system disturbances, such as power/current reference changes [21,22], line disconnections [23,24] and converter outages [20–23,25], has been discussed extensively in the current literature. Nevertheless, further research on post-event power distribution in MT-MVDC distribution systems is needed, taking into account the differences in network structure and operation mode between HVDC transmission and MVDC distribution systems.

This paper presents (*i*) a novel sequential PF algorithm for hybrid AC/MT-MVDC networks, utilizing a uniform MVDC bus type definition through a Fibonacci search-based NR (FSNR) approach, while considering the effect of VSCs and dc/dc converters on the whole PF; (*ii*) an accurate post-event power distribution analysis method to investigate the steady-state power distribution for droop-controlled MT-MVDC systems.

The proposed PF algorithm incorporates external HVAC/MVAC and embedded MVDC systems, while the HVAC and MVAC PF are derived, after the convergence of MVDC PF, by BFS and NR methods, respectively. Moreover, the FSNR MVDC PF computation method necessitates only the definition of the dc current bus, in addition to the slack bus. The original dc power buses in VSCs and dc/dc converters are transformed into dc current buses by estimating the initial dc current values within the power buses. These estimates are subsequently corrected using a modified Fibonacci search method [26], which incorporates the A^* algorithm [27] with heuristic search guide to enhance search efficiency when correcting multiple arrays of dc current values. The utilization of sequential method also enhances the integration of the presented FSNR MVDC PF algorithm with existing ac algorithms, ensuring the proposed sequential PF algorithm maintains robustness and efficacy, even with expanding system configurations.

The post-event power distribution analysis method proposed for MT-MVDC systems considers a widely adopted open-loop operation scheme with closed-loop design in distribution networks [28]. This approach ensures that the corresponding load terminals are initially isolated and interconnected during emergency conditions, thereby limiting fault current and providing power supply reliability [29,30]. The implementation of this scheme is dictated by the normally open (NO) or normally closed (NC) condition of tie switches (TSs) in switching stations [31]. Two generic closed loop operation modes are considered and tested in RTDS real-time digital simulators, including: (1) normal closed loop operation with multi-power source supply that TS is changed from NO condition to NC condition, and (2) closed loop operation after the outage of VSCs with power supply function. Dynamic I/V droop coefficients are further presented for VSCs and dc/dc converters using P/V droop control. This ensures accurate power redistribution

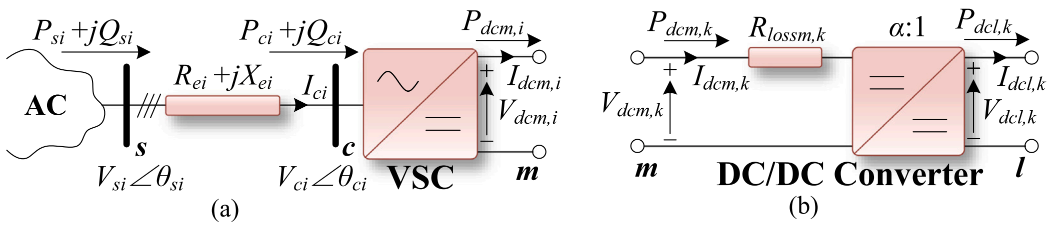

Fig. 1. VSC and dc/dc converter station models: (a) VSC, and (b) dc/dc converter.

calculations by directly correlating dc current and voltage, given that the deviation in dc current linearly corresponds to the dc voltage deviation.

In summary, the main contributions in this paper are:

1. MVDC and MVAC/HVAC PFs in a hybrid AC/MT-MVDC network are sequentially addressed using a novel proposed sequential PF algorithm. Moreover, the impacts of VSCs and dc/dc converters on the overall PF are explicitly introduced.
2. Bus type definition is simplified by the FSNR approach for the MVDC PF calculation where only the dc current bus type is considered. The MVDC PF calculation requires fewer iterations, as the Jacobian matrix remains constant.
3. Post-event power distribution is examined in detail for MT-MVDC distribution networks. This analysis is conducted under closed-loop operation, considering scenarios such as TS closure and the outage of sending-end VSCs along with their corresponding line disconnections.
4. Zero error power redistribution calculation is ensured by the FS method-based dynamic I/V droop coefficients. P/V droop coefficients for P/V droop controlled-converters are substituted by I/V droop coefficients to obtain a linear relationship between dc current and voltage deviation values.

The remainder of this article is structured in the following manner. Section 2 introduces the converter modeling and droop control description. Section 3 discusses the initial PF determination. The detailed power distribution analysis method under two operation modes is elaborated in Section 4, following with case studies in Section 4 for verifying the computation correctness and efficiency of expanded PF algorithm, and the accuracy of proposed power distribution analysis method. Section 5 draws the conclusion.

2. Converter modeling & droop control description

2.1. Converter modeling

In order to develop a detailed PF analysis considering HVAC, MVAC and MVDC networks, the modeling of generic VSCs and dc/dc converters will be first explored in this section. Simplified PF models are used to study the power losses of VSCs and dc/dc converters [17,32,33].

2.1.1. Voltage source converter

Fig. 1(a) shows the VSC station model including HVAC transmission or MVAC distribution system bus, converter bus, MVDC link and equivalent impedance of ac transformer ($R_{ei} + jX_{ei}$). The generalized power losses derivation method for VSC-based HVDC systems [34] can also be used in MVDC networks as:

$$P_{loss,ci} = C_{1,ci} + C_{2,ci} \cdot |I_{ci}| + C_{3,ci} \cdot |I_{ci}|^2, \tag{1}$$

where $C_{1,ci}$, $C_{2,ci}$, $C_{3,ci}$ represent the coefficients of no-load, linear, quadratic losses, and I_{ci} is the converter ac current which is calculated as:

$$I_{ci} = \sqrt{(P_{ci}^2 + Q_{ci}^2)/V_{ci}^2} = \sqrt{(P_{si}^2 + Q_{si}^2)/V_{si}^2}, \tag{2}$$

where P_{si}, Q_{si} and P_{ci}, Q_{ci} are the active power and reactive power at the grid side and converter side, respectively, V_{si} and V_{ci} refer to the corresponding voltages. Furthermore, the active power injected into the VSC is:

$$P_{ci} = P_{dcm,i} + P_{loss,ci} = V_{dcm,i} I_{dcm,i} + P_{loss,ci}, \tag{3}$$

where $V_{dcm,i}$ and $I_{dcm,i}$ are the dc voltage and dc current at the MVDC link, respectively. Moreover, the active/reactive power at the VSC bus can also be represented as:

$$\begin{cases} P_{ci} = P_{si} - R_{ei} \cdot (P_{si}^2 + Q_{si}^2)/V_{si}^2 \\ Q_{ci} = Q_{si} - X_{ei} \cdot (P_{si}^2 + Q_{si}^2)/V_{si}^2 \end{cases} \tag{4}$$

2.1.2. DC/DC converter

Dc/dc converters are used in an MVDC network to achieve dc voltage level change facilitating the access of different devices with dc interfaces. An equivalent dc/dc converter model is used as shown in Fig. 1(b) for simplifying the converter power loss analysis. The dc power at the medium voltage side (P_{dcm}) is expressed as (5), and the converter losses can be calculated as (6).

$$P_{dcm,k} = V_{dcm,k} I_{dcm,k} = P_{dcl,k} + P_{lossm,k}, \tag{5}$$

$$P_{lossm,k} = R_{lossm,k} \cdot I_{dcm,k}^2 = R_{lossm,k} \cdot (I_{dcl,k}/\alpha)^2, \tag{6}$$

where $R_{lossm,k}$ refers to the equivalent dc/dc converter resistance, and α is the transformation ratio.

2.2. Droop control description

A VSC in an MVDC system is able to achieve active and reactive power control functions. The active power control can be modeled into the control of (*i*) ac active power, (*ii*) dc power, (*iii*) dc current and (*iv*) dc voltage, while (*i*) reactive power control or (*ii*) ac voltage control can be realized in the reactive power control function [17]. Similar to the control modes in VSCs, dc current/power and dc voltage control can be adopted in the dc/dc converters to regulate the forward/reverse power and the dc voltage, respectively [5,35]. In addition, P/V or I/V droop control can be adopted in different VSC and dc/dc converters that all converters coordinate to balance the dc voltage in an MT-MVDC distribution system, hence the system reliability can be further improved.

When the VSCs in an MT-MVDC distribution system adopt droop control under steady-state operation, (7) can be established [17]. In addition, similar droop control expression can also be applied in dc/dc converters as (8) [11], and the dc power can be either in the LVDC or MVDC link.

$$\begin{cases} (P_{dcrefm,i}^{PV} - P_{dcm,i}^{PV}) + K_{droop,i}^{PV,vsc}(V_{dcrefm,i}^{PV} - V_{dcm,i}^{PV}) = 0 \\ (I_{dcrefm,i}^{IV} - I_{dcm,i}^{IV}) + K_{droop,i}^{IV,vsc}(V_{dcrefm,i}^{IV} - V_{dcm,i}^{IV}) = 0 \end{cases} \tag{7}$$

$$\begin{cases} P_{dcm/l,k}^{PV} + K_{droop,k}^{PV,dc/dc}(V_{dcm,k}^{PV} - V_{dcrefm,k}^{PV}) = 0 \\ I_{dcm,k}^{IV} + K_{droop,k}^{IV,dc/dc}(V_{dcm,k}^{IV} - V_{dcrefm,k}^{IV}) = 0 \end{cases} \tag{8}$$

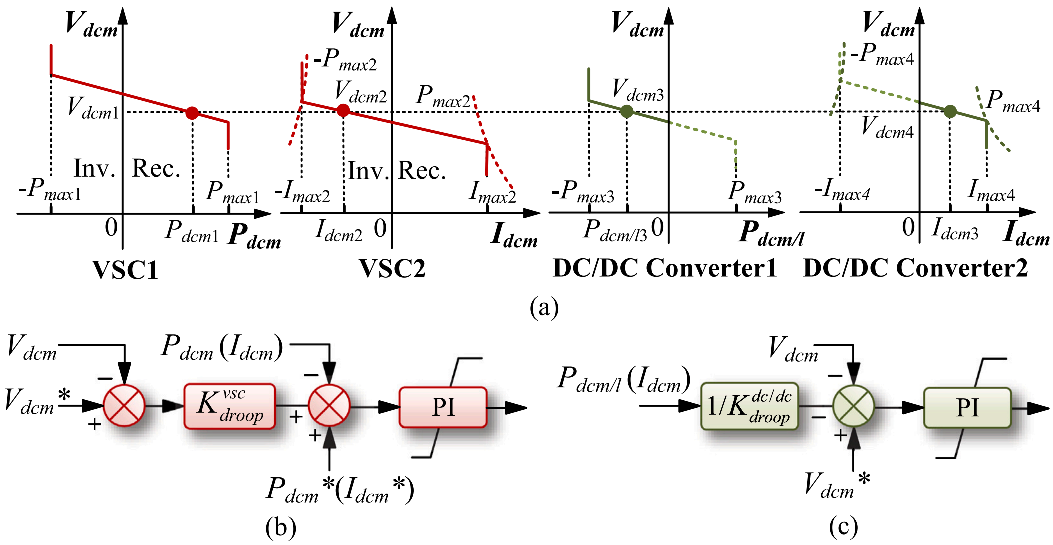

Fig. 2. Static characteristic of droop control in MT-MVDC distribution systems: (a) P/V and I/V droop control in VSCs and dc/dc converters, (b) structure of droop controller in the VSC, and (c) structure of droop controller in the dc/dc converter.

Eqs. (9) and (10) for VSCs can be further derived when dc power/ current and dc voltage deviations ($\Delta x_{dci} = x_{dci} - x^0_{dci}$) are considered after different system disturbances.

$$\Delta P^{PV}_{dcm,i} - \Delta P^{PV}_{dcrefm,i} = K^{PV,vsc}_{droop,i}(\Delta V^{PV}_{dcrefm,i} - \Delta V^{PV}_{dcm,i}) \tag{9}$$

$$\Delta I^{IV}_{dcm,i} - \Delta I^{IV}_{dcrefm,i} = K^{IV,vsc}_{droop,i}(\Delta V^{IV}_{dcrefm,i} - \Delta V^{IV}_{dcm,i}) \tag{10}$$

Similarly, (11) and (12) can also be obtained in dc/dc converters.

$$\Delta P^{PV}_{dcm/l,k} = K^{PV,dc/dc}_{droop,k}(\Delta V^{PV}_{dcrefm,k} - \Delta V^{PV}_{dcm,k}) \tag{11}$$

$$\Delta I^{IV}_{dcm,k} = K^{IV,dc/dc}_{droop,k}(\Delta V^{IV}_{dcrefm,k} - \Delta V^{IV}_{dcm,k}) \tag{12}$$

The droop constants for P/V and I/V droop control can be defined as (13) and (14), respectively [22].

$$K^{PV}_{droop} = (V_{dcm,rated}\delta_{droop})^{-1}P_{dc,rated}\ (\mathrm{MW/kV}), \tag{13}$$

$$K^{IV}_{droop} = (V^2_{dcm,rated}\delta_{droop})^{-1}P_{dc,rated}\ (\mathrm{kA/kV}), \tag{14}$$

where $P_{dc,rated}$ and $V_{dcm,rated}$ is the rated dc power and rated MVDC voltage of each converter, respectively, and δ_{droop} refers to the maximum allowable dc voltage deviation ratio [25]. Fig. 2 shows the static characteristic of droop control in a four-terminal MVDC distribution system considering VSCs and dc/dc converters. The dc power/current and voltage in VSCs and dc/dc converters after different system disturbances would deviate according to respective droop characteristics. The detailed analysis will be elaborated in Section 4.

3. Initial power flow determination

In the proposed hybrid AC/MT-MVDC PF algorithm, the ac PF of the connected HVAC/MVAC grid is solved after obtaining the MVDC PF by a sequential method. The PF equations of VSCs and dc/dc converters are included in the MVDC PF computation. Moreover, a novel FSNR dc PF algorithm is proposed to simplify bus type definition and avoid the solution of multiple sub-Jacobian matrices in the MVDC PF calculation. Single dc current bus type is employed by assuming the type of dc power bus to be dc current bus. The additional P/V and I/V droop buses [15,17] are respectively considered as dc power and current buses in this section, owing to the similarity of Jacobian matrices. The proposed PF algorithm inherits the convergence performance as the conventional NR algorithm, since all initial values are constant in each search step.

3.1. MVDC power flow

Multi-initial dc power and/or current values are known in VSCs and dc/dc converters with constant dc power, current and droop control modes. When the dc current at the LV side of a dc/dc converter is a known value, the dc current at the MV side can be derived by the transformation ratio ($I_{dcm,k} = I_{dcl,k}/\alpha$). However, the dc power at the MV side of a dc/dc converter cannot be obtained directly with known dc power value at the LV side if the converter losses cannot be ignored. In order to initialize the MVDC PF, the dc power at the MV side is first assumed to be the corresponding dc power value at the LV side as:

$$P_{dcm,k(0)} = P_{dcl,k}, \tag{15}$$

where subscript (0) refers to the initial values of the corresponding MVDC buses.

One dc voltage (the first VSC-connected bus is assumed to be a slack bus), f dc power and g dc current are known values to initialize the MVDC PF. The MVDC PF can be solved by the conventional NR method, obtaining $n-1$ dc voltages [25]. Only dc power or current bus is defined in the case of $f = 0$ or $g = 0$. However, it is necessary to define two types of buses (dc power and current buses) when $f \neq 0$ and $g \neq 0$ in conventional dc PF solving algorithm, and multiple sub-Jacobian matrices have to be constructed and solved [25]. In order to simplify the definition of different types of buses and the solution of multiple Jacobian matrices, a single dc current bus-based FSNR approach is presented to solve the MVDC PF with the initial condition of one dc voltage and multiple dc power or current. The dc current injected to dc buses with one known dc voltage and $n-1$ known or estimated dc currents can be expressed as:

$$\begin{cases} I_{dcm,1} = \sum_{j=1}^{n} G_{dcm_{1j}}V_{dcm,j}, \\ I_{dcm,i} = \sum_{j=1}^{n} G_{dcm_{ij}}V_{dcm,j}\ (i = 2, 3, \ldots, n), \end{cases} \tag{16}$$

where G_{dcm} is line conductance. The relationship between column vector $\boldsymbol{\Delta I_{dcm}}$ and $\boldsymbol{\Delta V_{dcm}}$ can be established by mismatch Eqs. (18) based on (16) and (17).

$$\Delta I_{dcm,i} = I_{dcm,i} - \sum_{j=1}^{n} G_{dcm_{ij}}V_{dcm,j} = 0 \tag{17}$$

$$\boldsymbol{\Delta I_{dcm}} = \boldsymbol{J^I_{dcm}}\boldsymbol{\Delta V_{dcm}} = \boldsymbol{G_{dcm}}\boldsymbol{\Delta V_{dcm}} \tag{18}$$

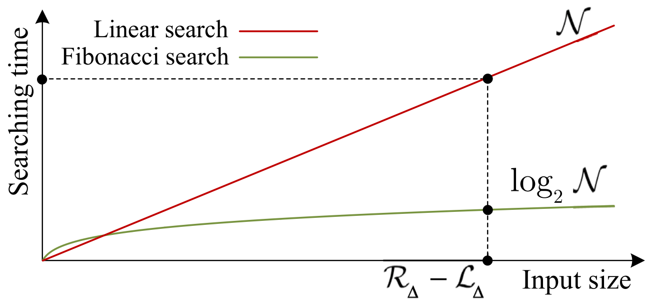

Fig. 3. Time complexity of Fibonacci search method.

Moreover, less number of iterations is required for the dc current bus type-based MVDC PF calculation, since the Jacobian matrix $\boldsymbol{J}^{I}_{dcm}$ is constant in the iteration process. Two stage calculation is employed in the proposed FSNR dc PF algorithm.

3.1.1. Current estimation stage (stage 1)

In stage 1 (current estimation), the dc current for converter u with known dc power is estimated as (19) when a single dc current-based bus type is used.

$$I^{est}_{dcm,u} = \frac{P^{pre}_{dcm,u}}{V_{dcm,rated}}, \tag{19}$$

where $P^{pre}_{dcm,u}$ is the pre-specified dc power values for certain VSCs and dc/dc converters. In the following stage (stage 2), correction iteration is conducted since there is a dc current deviation ($\Delta I^{cor}_{dcm,u}$) between the estimated and actual dc current u. Hence, the actual dc current can be expressed as:

$$I^{act}_{dcm,u} = I^{est}_{dcm,u} + \Delta I^{cor}_{dcm,u} = \frac{P^{pre}_{dcm,u}}{V_{dcm,rated}} + \Delta I^{cor}_{dcm,u}, \tag{20}$$

where $\Delta I^{cor}_{dcm,u} = 0$ in the initial external iteration leading to $I^{act}_{dcm,u(0)} = I^{est}_{dcm,u}$. It is worth noting that the convergence of the internal NR algorithm is not affected by the external FS algorithm, since $I^{act}_{dcm,u}$ maintains a constant value during each search step.

3.1.2. Current correction iteration stage (stage 2)

In the correction iteration stage, a modified Fibonacci search method is employed to obtain the accurate dc current values. The Fibonacci search is an improved binary search method, which can reduce the number of total correction iterations due to its logarithmic time complexity ($\mathcal{O}(\log_2 \mathcal{N})$, $\mathcal{N}$ is input size) in the worst case as shown in Fig. 3. Moreover, the best-case performance of Fibonacci search is $\mathcal{O}(1)$ [26].

Fig. 4(a) and (b) show the Fibonacci global array based Fibonacci number ($\mathcal{F}ibo(\mathcal{N}')$) and element distribution, respectively. It is essential to confirm that the search algorithm remains effective when simultaneously conducting searches across multiple arrays (estimated dc current values). The proposed FSNR approach utilizes a modified Fibonacci search scheme, in which the A^* algorithm [27] initially executes the value closest to the target to expedite the search process when multiple values need correction, as illustrated in Fig. 4(c). The search range is obtained by the maximum allowable dc current deviation for the terminal u with known dc power, which is determined by the dc voltage deviation ratio δ_{droop}. Thus, the left and right margins for MV terminals are defined as (21), and the middle value $\mathcal{M}_{\Delta I_{m,u}}$ in each searching step should follow (22).

$$\begin{cases} \mathcal{L}_{\Delta I_{m,u}} = \dfrac{-P^{pre}_{dcm,u}\delta_{droop}}{V_{dcm,rated}(1+\delta_{droop})} \\ \mathcal{R}_{\Delta I_{m,u}} = \dfrac{P^{pre}_{dcm,u}\delta_{droop}}{V_{dcm,rated}(1-\delta_{droop})} \end{cases} \tag{21}$$

$$\mathcal{M}_{\Delta I_{m,u}} = \mathcal{L}_{\Delta I_{m,u}} + \mathcal{F}ibo(\mathcal{N}'-1) - 1 \tag{22}$$

The accurate dc current for certain VSCs and dc/dc converters with known dc power can be derived by setting the known dc power as iteration target values ($P^{pre}_{dcm,u} = P^{tar}_{dcm,u}$). If the deviations between the target values and obtained dc power are acceptable as (23), the corresponding dc currents in (16) will be substituted by the corrected values.

$$\|\boldsymbol{\Psi}_u\|_\infty < \varepsilon_p, \text{ and} \tag{23}$$

$$\boldsymbol{\Psi}_u = [P^{tar}_{dcm,1} - I^{act}_{dcm,1}V^{act}_{dcm,1}, \dots, P^{tar}_{dcm,u} - I^{act}_{dcm,u}V^{act}_{dcm,u}]^{-1}.$$

In addition, the dc power at MV sides of dc/dc converters should be updated if the initial dc power values at the LV sides are known when considering converter losses. The current dc power deviation at the LVDC buses of dc/dc converters is calculated as:

$$\Delta P_{dcl,k(0)} = P_{dcm,k(0)} - P_{lossm,k(0)} - P_{dcl,k(0)}, \tag{24}$$

then $\Delta P_{dcl,k(0)}$ is added to $P_{dcm,k(0)}$ as (25) to update the dc power values at MVDC buses.

$$P_{dcm,k(1)} = P_{dcm,k(0)} - \Delta P_{dcl,k(0)} \tag{25}$$

The MVDC PF is finally solved when $\Delta P_{dcl,k}$ is in the scope of acceptance as:

$$\begin{cases} \Delta P_{dcl,k(n)} = P_{dcm,k(n)} - P_{lossm,k(n)} - P_{dcl,k(n)} \\ P_{dcm,k(n+1)} = P_{dcm,k(n)} - \Delta P_{dcl,k(n)}. \end{cases} \tag{26}$$

Following the algorithm flowchart in the left box of Fig. 5, the MVDC PF for MT-MVDC systems is finally solved.

3.2. HVAC and MVAC power flow

In the proposed sequential AC/MT-MVDC PF algorithm, the HVAC or MVAC grid PF is computed following the convergence of MVDC PF. Conventional NR and BFS PF methods [7,13] are employed to solve the ac PF of connected HVAC transmission systems and MVAC distribution networks, respectively. Unlike the ring structure-based HVAC transmission systems, MVAC distribution systems primarily consist of radial structures, in which there is a single path from the source to any load bus. Additionally, MVAC distribution systems serve as secondary networks that distribute power from connected HVAC or MVDC systems through ac substations. Consequently, an MVAC distribution network can be considered an equivalent ac load for the interconnected HVAC and MVDC systems (Fig. 6).

The MVAC PF can be effectively addressed using the conventional BFS method, where the backward and forward sweep processes accurately adjust currents and voltages, respectively [7]. In the backward process, voltage vector $\boldsymbol{V}_r$ and current vector $\boldsymbol{I}_{r,in}$ at the MVAC bus r are used to derive voltage vector $\boldsymbol{V}_l$ and current vector $\boldsymbol{I}_{l,out}$ at the MVAC bus l (Fig. 7) as:

$$\begin{cases} \boldsymbol{V}_l = (\boldsymbol{Y}^{rl}_{r,br})^{-1}(\boldsymbol{I}_{r,in} - \boldsymbol{Y}^{rr}_{r,br}\boldsymbol{V}_r), \\ \boldsymbol{I}_{l,out} = \boldsymbol{Y}^{ll}_{r,br}\boldsymbol{V}_l + \boldsymbol{Y}^{lr}_{r,br}\boldsymbol{V}_r, \\ \boldsymbol{I}_{r,in} = \boldsymbol{I}_{br,in} - \boldsymbol{I}_{br,out} - \boldsymbol{I}_{r,out}, \end{cases} \tag{27}$$

where $\boldsymbol{Y}_{r,br}$ is the admittance matrix of branch r. Moreover, voltage vector $\boldsymbol{V}_l$ and current vector $\boldsymbol{I}_{l,out}$ at the MVAC bus l are then used to update the values of voltage vector $\boldsymbol{V}_r$ and current vector $\boldsymbol{I}_{r,in}$ at the MVAC bus r in the forward sweep process following:

$$\begin{cases} \boldsymbol{V}_r = (\boldsymbol{Y}^{lr}_{r,br})^{-1}(\boldsymbol{I}_{l,out} - \boldsymbol{Y}^{ll}_{r,br}\boldsymbol{V}_l), \\ \boldsymbol{I}_{r,in} = \boldsymbol{Y}^{rr}_{r,br}\boldsymbol{V}_r + \boldsymbol{Y}^{rl}_{r,br}\boldsymbol{V}_l, \\ \boldsymbol{I}_{r,out} = \boldsymbol{I}_{br,in} - \boldsymbol{I}_{br,out} - \boldsymbol{I}_{r,in}. \end{cases} \tag{28}$$

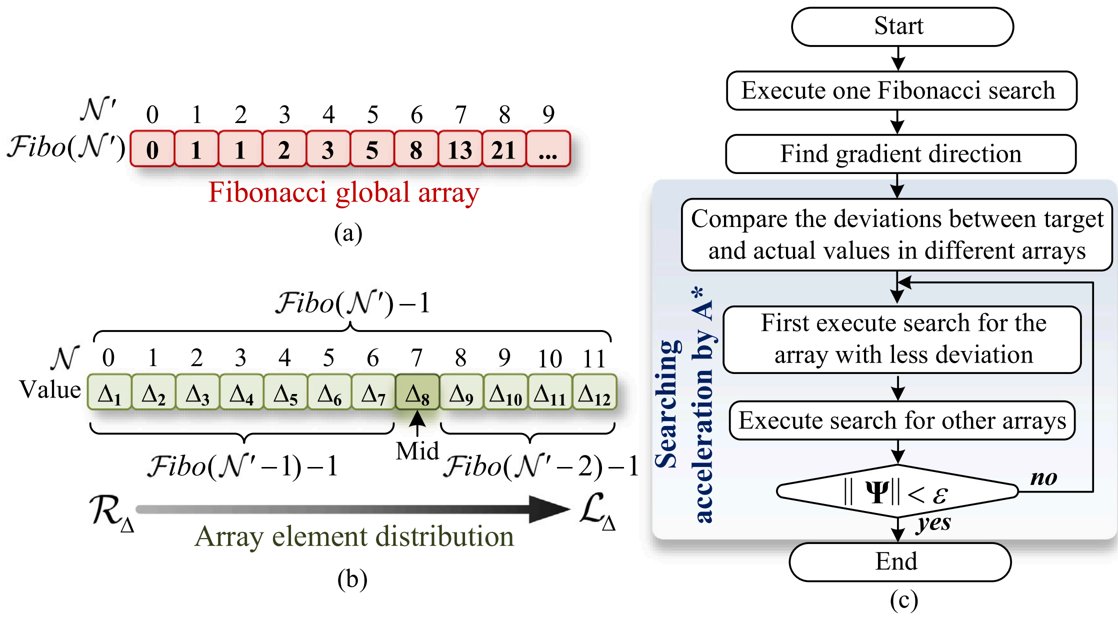

Fig. 4. Modified Fibonacci search method: (a) Fibonacci global array, (b) array element distribution, and (c) flowchart of the modified Fibonacci search scheme.

In the HVAC transmission systems, the active/reactive power equations in HVAC buses are respectively expressed as:

$$\begin{cases} P_{ge,i} - P_{lo,i} - \xi P_{si} - \zeta P'_{si} - V_i \sum_{j=1}^{n} V_j (G_{ij} \times \\ \cos\theta_{ij} + B_{ij}\sin\theta_{ij}) = 0, \\ Q_{ge,i} - Q_{lo,i} - \xi Q_{si} - \zeta Q'_{si} - V_i \sum_{j=1}^{n} V_j (G_{ij} \times \\ \sin\theta_{ij} - B_{ij}\cos\theta_{ij}) = 0, \end{cases} \tag{29}$$

where $P_{ge,i}$ and $Q_{ge,i}$ are active and reactive power of generators at HVAC bus i, $P_{lo,i}$ and $Q_{lo,i}$ are active and reactive power of connected loads, P'_{si} and Q'_{si} are total consumed active and reactive power from connected MVAC distribution systems at HVAC bus i (Fig. 6(a)). Coefficient ξ or $\zeta = 1$ and ξ or $\zeta = 0$ refer to the HVAC buses with and without connection of VSCs or MVAC distribution systems, respectively.

In the HVAC PF derivation process, the injected/consumed active/reactive power (P_{si}, P'_{si}, Q_{si}, Q'_{si}) from MVDC and MVAC distribution networks at HVAC buses should be acquired first. The reactive power Q_{si} can be obtained directly when VSCs adopt constant Q_{si} control, or adapts the reactive power output by a constant ac voltage (V_{si}) control mode [17]. In addition, the active and reactive power at HVAC bus i from connected MVAC systems can be derived from:

$$\begin{cases} P'_{si} = P_{di} + R'_{ei} \cdot (P_{di}^2 + Q_{di}^2)/V_{di}^2, \\ Q'_{si} = Q_{di} + X'_{ei} \cdot (P_{di}^2 + Q_{di}^2)/V_{di}^2. \end{cases} \tag{30}$$

Although the accurate active power P_{si} cannot be directly obtained, it can be first estimated to be the MVDC power $P_{dcm,i}$ and will be updated from the up-to-date HVAC PF [15]. The detailed MVAC and HVAC PF calculation flowchart is shown in the right part of Fig. 5.

4. Power distribution analysis under different operating modes

Similar to ac distribution systems, MVDC distribution networks can also adopt the scheme of open-loop operation with closed-loop design [29] that corresponding MVDC terminals are initially isolated and connected together by TSs for allowing power supply of all loads after certain power failures [31]. Two generic closed-loop operation modes for MVDC distribution systems are considered in this section, including (*i*) normal closed-loop operation with multi-power source supply (operation mode 1 - Fig. 8(a)), and (*ii*) closed-loop operation after the outage of VSCs with power supply function (operation mode 2 - Fig. 8(b)). The proposed power redistribution analysis method only considers the relationship between dc current and voltage by the introduction of dynamic I/V droop coefficients, even when mixed P/V and I/V droop control schemes coexist within the same system. This approach allows for precise power redistribution calculations, given the linear relationship between dc current and voltage deviations.

4.1. Generic closed-loop operation mode 1: Normal operation with multi-power source supply

Assuming TSs are open in the initial operation state (open-loop operation), the power would be redistributed within the MVDC network after closing the TS. All TS-connected MVDC buses have identical voltages, when TSs are closed in one switching station, if ignoring the losses of switches.

It can be considered there is very small resistance between different TS-connected MVDC buses [31], hence the (*i*) system conductance $G_{dcm,ij}$ and (*ii*) network current distribution are changed together. The network currents are redistributed after the closing of TSs. The initial MVDC terminal current without closing TSs is:

$$I_{dcm,i}^{ini} = I_{line,i1}^{ini} + I_{line,i2}^{ini} + \cdots + I_{line,in}^{ini}, \tag{31}$$

where $I_{line,ij} = -(V_{dcm,i} - V_{dcm,j})G_{dcm,ij}$ ($j = 1, 2, \ldots, n$ and $j \neq i$). The terminal currents after closing TSs are expressed as (32) if a TS between MVDC buses i and h is closed. Thus, the terminal current deviations (33) are calculated by subtraction from (31) from (32), and (33) can be further expressed as (34).

$$I_{dcm,i}^{tc} = I_{line,i1}^{tc} + I_{line,i2}^{tc} + \cdots + I_{line,in}^{tc} + I_{tie,ih} \tag{32}$$

$$\Delta I_{dcm,i} = \Delta I_{line,i1} + \Delta I_{line,i2} + \cdots + \Delta I_{line,in} + I_{tie,ih} \tag{33}$$

$$\begin{aligned} &\Delta I_{dcm,i} + (V_{dcm,i}^{ini} - V_{dcm,h}^{ini})G_{dcm,ih} = J_{dcm,ii}^{I,tc}\Delta V_{dcm,i} + \\ &J_{dcm,ij}^{I,tc}\Delta V_{dcm,j} = G_{dcm,ii}^{tc}\Delta V_{dcm,i} + G_{dcm,ij}^{tc}\Delta V_{dcm,j} \\ &(j = 1, 2, 3, \ldots, n, h \text{ and } j \neq i) \end{aligned} \tag{34}$$

The TS branch conductance between MVDC buses i and h is also included in (34), hence the dc current deviation vector $\boldsymbol{\Delta I_{dcm}}$ in (18)

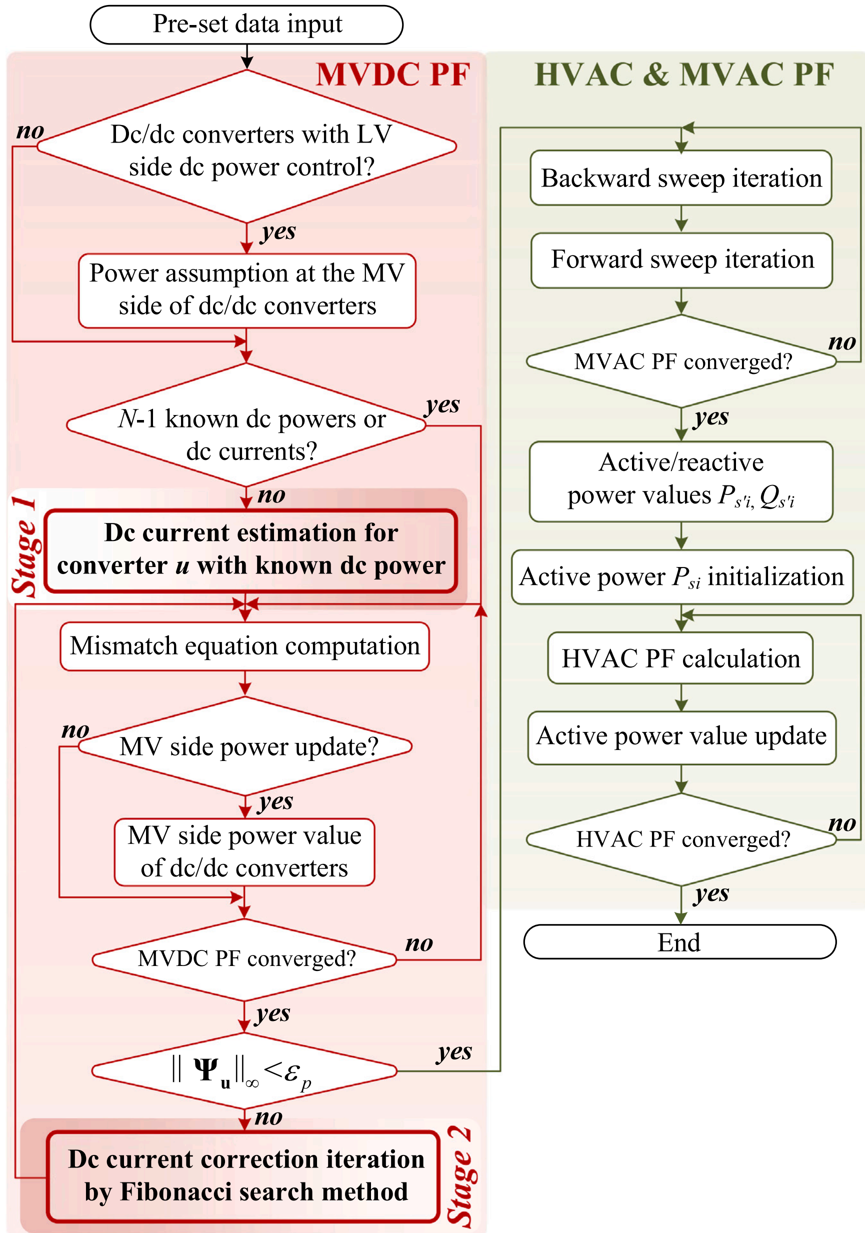

Fig. 5. Flowchart of proposed sequential hybrid AC/MT-MTDC PF algorithm.

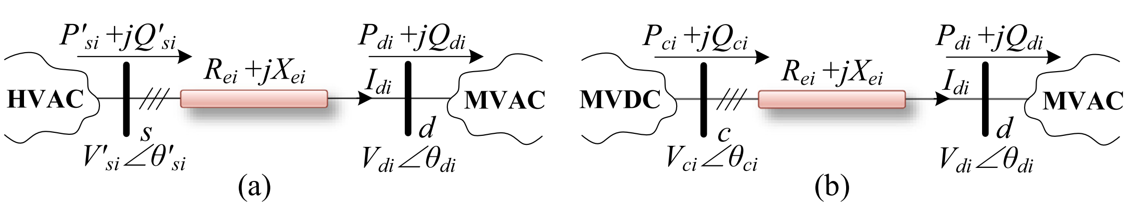

Fig. 6. HVAC-MVAC and MVDC-MVAC network link: (a) HVAC-MVAC network link, and (b) MVDC-MVAC network link.

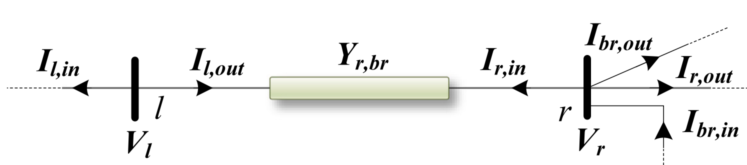

Fig. 7. A feeder in an MVAC distribution system.

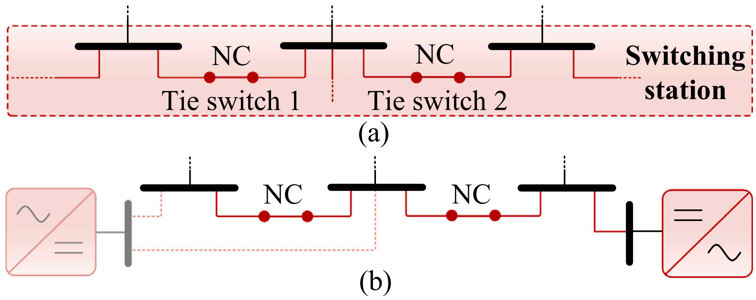

Fig. 8. Two generic closed-loop operation modes in MVDC systems: (a) generic closed-loop operation mode 1, and (b) generic closed-loop operation mode 2.

should be replaced by:

$$\boldsymbol{\Delta I}_{dcm} + \epsilon_{tc}(\boldsymbol{V}^{ini}_{dcm,\nu} - \boldsymbol{V}^{ini}_{dcm,\kappa})\boldsymbol{G}_{dcm,\nu\kappa} = \boldsymbol{\Delta I}_{dcm} + \boldsymbol{\mathcal{A}}, \tag{35}$$

where $\boldsymbol{\mathcal{A}} = \epsilon_{tc}(\boldsymbol{V}^{ini}_{dcm,\nu} - \boldsymbol{V}^{ini}_{dcm,\kappa})\boldsymbol{G}_{dcm,\nu\kappa}$, $\boldsymbol{V}^{ini}_{dcm}$ and $\boldsymbol{G}_{dcm,\nu\kappa}$ are column vectors, ν and κ refer to the connected MVDC buses of TSs, $\epsilon_{tc} = 1$ means the corresponding TSs are closed, while $\epsilon_{tc} = 0$ shows no corresponding TSs closing. Due to no deviations of dc voltage and dc current references ($\Delta V_{dcrefm} = 0$, $\Delta I_{dcrefm} = 0$) after closing TSs, (9)–(12) can be further simplified as (36) to (39), respectively.

$$\Delta P^{PV}_{dcm,i} = -K^{PV,vsc}_{droop,i}\Delta V^{PV}_{dcm,i} \tag{36}$$

$$\Delta I^{IV}_{dcm,i} = -K^{IV,vsc}_{droop,i}\Delta V^{IV}_{dcm,i} \tag{37}$$

$$\Delta P^{PV}_{dcm/l,k} = -K^{PV,dc/dc}_{droop,k}\Delta V^{PV}_{dcm,k} \tag{38}$$

$$\Delta I^{PV}_{dcm,k} = -K^{IV,dc/dc}_{droop,k}\Delta V^{IV}_{dcm,k} \tag{39}$$

Furthermore, the dc voltage and dc current deviations in all MVDC buses can be calculated as (40) by combining (14), (18), (35), (37), (39) if only I/V droop control is adopted for all VSCs and dc/dc converters. Moreover, the dc power deviation $\boldsymbol{\Delta P}^{tc}_{dcm}$ can be further derived.

$$\begin{cases} \boldsymbol{\Delta V}^{IV,tc}_{dcm} = (\mathrm{diag}(\boldsymbol{K}^{IV}_{droop}) + \boldsymbol{G}^{tc}_{dcm})^{-1}\boldsymbol{\mathcal{A}} \\ \boldsymbol{\Delta I}^{IV,tc}_{dcm} = -\mathrm{diag}(\boldsymbol{K}^{IV}_{droop})\boldsymbol{\Delta V}^{IV,tc}_{dcm} \end{cases} \tag{40}$$

A matrix invertibility examination procedure (Fig. 9) is utilized to ensure the calculation effectiveness under the initially assumed resistance $R_{ts,ini}$. The invertibility of the matrix $(\mathrm{diag}(\boldsymbol{K}^{IV}_{droop}) + \boldsymbol{G}^{tc}_{dcm})$ in (40) is examined by assessing its rank. In cases where the matrix is non-invertible, the TS resistance R_{ts} is sequentially increased by a factor of ten.

Since (40) cannot solve the power distribution for certain converters with P/V droop control or constant dc power control, a dynamic I/V droop coefficient $\mathcal{K}^{IV,pv}_{droop}$ is introduced and defined as (41), which also serves the operation mode 2. The dc current/voltage deviations can be first derived by (40) with estimated I/V droop constant ($K^{IVest,pv}_{droop,\tau} = K^{PV}_{droop,\tau}/V_{dcm,rated}$) for P/V droop controlled-VSC or dc/dc converter τ. It should be noted that $K^{IVest,pv}_{droop,\tau} = 0$ for converter τ with constant dc power control.

$$\mathcal{K}^{IV,pv}_{droop} = K^{IVest,pv}_{droop} + \Delta K^{IV,pv}_{droop}, \tag{41}$$

and the left and right margins are:

$$\begin{cases} \mathcal{L}_{\Delta\mathcal{K}^{IV,pv}_{droop}} = \dfrac{-(\vartheta K^{IVest,pv}_{droop} + \Theta K^{IVvir,pv}_{droop})\delta_{droop}}{1 + \delta_{droop}} \\ \mathcal{R}_{\Delta\mathcal{K}^{IV,pv}_{droop}} = \dfrac{(\vartheta K^{IVest,pv}_{droop} + \Theta K^{IVvir,pv}_{droop})\delta_{droop}}{1 - \delta_{droop}}, \end{cases} \tag{42}$$

where a virtual droop constant $K^{IVvir,pv}_{droop}$ is defined ($K^{IVvir,pv}_{droop} = (V^2_{dcm,rated}\delta_{droop})^{-1}P_{dc,rated}$) for a VSC or dc/dc converter with constant dc power control, $\vartheta = 1 - \Theta = 1$ and 0 refer to a VSC or dc/dc converter with P/V droop control and constant dc power control, respectively.

The dc power, current and voltage deviations will be changed with the variation of $\mathcal{K}^{IV,pv}_{droop}$. In addition, the actual droop constant for P/V droop controlled converters can also be expressed as (43) from (36) and (38).

$$\begin{cases} K^{PV,vsc}_{droop,i} = -\Delta P^{PV}_{dcm,i}/\Delta V^{PV}_{dcm,i} \\ K^{PV,dc/dc}_{droop,k} = -\Delta P^{PV}_{dcm/l,k}/\Delta V^{PV}_{dcm,k} \end{cases} \tag{43}$$

The Fibonacci search method is used in the range of $[\mathcal{L}_{\Delta\mathcal{K}^{IV,pv}_{droop}}, \mathcal{R}_{\Delta\mathcal{K}^{IV,pv}_{droop}}]$ to find a proper $\mathcal{K}^{IV,pv}_{droop,\tau}$ that satisfies:

$$\|\boldsymbol{\Psi}_{\tau}\|_{\infty} < \varepsilon_{k,tc}, \text{ and} \tag{44}$$

$\boldsymbol{\Psi}_{\tau} = [K^{PV,tar}_{droop,1} + \frac{\Delta P_{dcm/l,1}}{\Delta V_{dcm,1}}, \ldots, K^{PV,tar}_{droop,o} + \frac{\Delta P_{dcm/l,o}}{\Delta V_{dcm,\tau}}]^{-1}$, where $K^{PV,tar}_{droop}$ is the pre-specified droop constant for VSC or dc/dc converter with P/V droop control. Following the flowchart in the left box of Fig. 10, the power distribution for an MT-MTDC distribution system under mixed P/V and I/V droop control after TSs closing can be finally derived.

4.2. Generic closed-loop operation mode 2: Operation after the outage of VSCs with power supply function

Under the normal closed-loop operation mode, ac and dc loads in an MVDC system are supplied by multiple sources ensuring at least $N-1$ safety principles. The remaining VSCs with power supply mode still have the capability to deliver power to all loads by closing corresponding TSs after the outage of certain VSCs. The power distribution calculation after the possible outage of VSCs with power supply function can be divided into three stages: (*i*) TS closing, (*ii*) converter outage, and (*iii*) line disconnection. This process is executed in a sequential manner, beginning with Stage 1 and progressing through to Stage 3.

4.2.1. TS closing (stage 1)

It is necessary to close corresponding TSs when certain VSCs with the power supply function quit operation for avoiding load power failure. Following the calculation process in Section 4.1, the dc power/current and voltage deviations when corresponding TSs are in the NC state can be obtained, which is the first calculation stage. Moreover, the current dc power/current and voltage in all terminals are used in the next calculation stage.

4.2.2. Converter outage (stage 2)

The outage of the source-connected VSC υ under P/V or converter ω under I/V droop control in an MVDC system can be summarized as:

$$\begin{cases} \Delta P^{PV}_{dcrefm,\upsilon} = -P^{PV}_{dcm,\upsilon}, \\ K^{PV}_{droop,\upsilon} = 0, \end{cases} \tag{45}$$

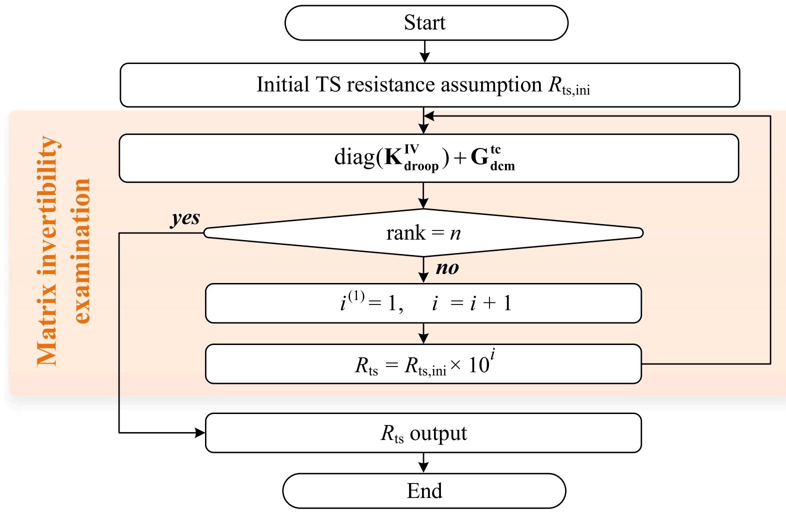

Fig. 9. Matrix invertibility checking procedure after closing TSs.

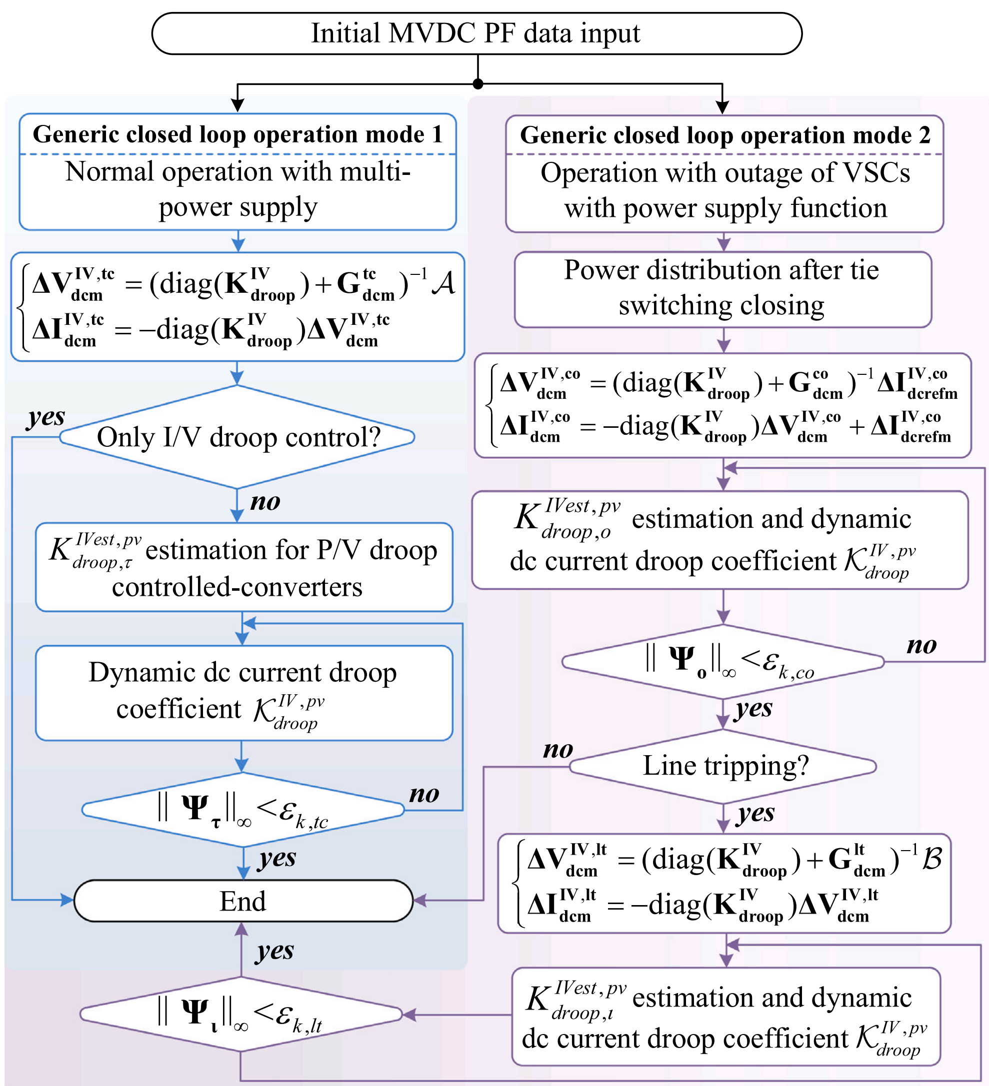

Fig. 10. Flowchart of the proposed power distribution analysis method in MT-MVDC systems under two operation modes.

or

$$\begin{cases} \Delta I_{dcrefm,\omega}^{IV} = -I_{dcm,\omega}^{IV}, \\ K_{droop,\omega}^{IV} = 0. \end{cases} \quad (46)$$

Supposing $\Delta V_{dcrefm} = 0$, (9) and (10) are simplified as (47), (48), (38), (39), respectively.

$$\Delta P_{dcm,i}^{PV} - \Delta P_{dcrefm,i}^{PV} = -K_{droop,i}^{PV,vsc} \Delta V_{dcm,i}^{PV} \quad (47)$$

$$\Delta I_{dcm,i}^{IV} - \Delta I_{dcrefm,i}^{IV} = -K_{droop,i}^{IV,vsc} \Delta V_{dcm,i}^{IV} \quad (48)$$

If all VSCs and dc/dc converters are with I/V droop control, (49) can be obtained by combining (14), (18), (39), (48), and the power distribution can be derived by replacing (46) into (49).

$$\begin{cases} \boldsymbol{\Delta V}_{dcm}^{IV,co} = (\mathrm{diag}(\boldsymbol{K}_{droop}^{IV}) + \boldsymbol{G}_{dcm}^{co})^{-1} \boldsymbol{\Delta I}_{dcrefm}^{IV,co} \\ \boldsymbol{\Delta I}_{dcm}^{IV,co} = -\mathrm{diag}(\boldsymbol{K}_{droop}^{IV}) \boldsymbol{\Delta V}_{dcm}^{IV,co} + \boldsymbol{\Delta I}_{dcrefm}^{IV,co} \end{cases} \quad (49)$$

In order to calculate the power distribution under mixed P/V and I/V droop control, the dynamic coefficient $\mathcal{K}_{droop}^{IV,pv}$ is also used in this stage, while the droop constant for P/V droop control after converter outage should also follow (43) from (38) and (47) due to $\Delta P_{dcrefm,i}^{PV} = 0$. Similarly, a proper $\mathcal{K}_{droop,o}^{IV,pv}$ can be found by the Fibonacci search method in the range of $[\mathcal{L}_{\mathcal{K}_{droop}^{IV,pv}}, \mathcal{R}_{\mathcal{K}_{droop}^{IV,pv}}]$ that meet:

$$\|\boldsymbol{\Psi}_o\|_\infty < \varepsilon_{k,co}, \text{ and} \quad (50)$$

$\boldsymbol{\Psi}_o = [K_{droop,1}^{PV,tar} + \frac{\Delta P_{dcm/l,1}}{\Delta V_{dcm,1}}, \ldots, K_{droop,1}^{PV,tar} + \frac{\Delta P_{dcm/l,o}}{\Delta V_{dcm,o}}]^{-1}$ for VSC or dc/dc converter o with P/V droop control.

4.2.3. Line disconnection (stage 3)

The system conductance matrix and network current distribution would change after any line disconnection. However, tripping of lines connected to the isolated VSCs is not included in calculation Stage 2. Therefore, the power distribution calculation after line disconnection is conducted in this stage.

It should be noted that the isolated converter terminals are not included in the following calculations. Eq. (51) shows the derived terminal currents in stage 2. The terminal currents after line tripping are expressed as (52) if a line between terminals i and g is tripped. Thus, the terminal current deviations (53) are calculated by subtracting (51) from (52).

$$I_{dcm,i}^{co} = I_{line,i1}^{co} + \cdots + I_{line,ig}^{co} + \cdots + I_{line,in}^{co} + I_{tie,ih}^{co} \quad (51)$$

$$I_{dcm,i}^{trip} = I_{line,i1}^{trip} + \cdots + 0 + \cdots + I_{line,in}^{trip} + I_{tie,ih}^{trip} \quad (52)$$

$$\Delta I_{dcm,i} = \Delta I_{line,i1} + \cdots - I_{line,ig}^{co} + \cdots + \Delta I_{line,in} + \Delta I_{tie,ih} \quad (53)$$

Similar to the derivation of (34), (53) can also be expressed as (54), which does not include the line conductance G_{ig}.

$$\Delta I_{dcm,i} + I_{line,ig}^{co} = G_{dcm,ii}^{lt} \Delta V_{dcm,i} + G_{dcm,ij}^{lt} \Delta V_{dcm,j} \quad (j \neq i \text{ and } j \neq g) \quad (54)$$

Therefore, (55) should be used in the calculation of Stage 3.

$$\boldsymbol{\Delta I}_{dcm} + \epsilon_{lt} \boldsymbol{I}_{line,\lambda\mu}^{co} = \boldsymbol{\Delta I}_{dcm} + \boldsymbol{\mathcal{B}} \quad (55)$$

where $\boldsymbol{\mathcal{B}} = \epsilon_{lt} \boldsymbol{I}_{line,\lambda\mu}^{co}$, λ and μ refer to the connected MVDC buses of tripped lines, $\epsilon_{lt} = 1$ means the corresponding lines are tripped, while $\epsilon_{lt} = 0$ shows no corresponding line tripping. The voltage and current deviations in all terminals at Stage 3 can be calculated as (56), if all VSCs and dc/dc converters adopt I/V droop control, by combining (14), (18), (37), (39), (55).

$$\begin{cases} \boldsymbol{\Delta V}_{dcm}^{IV,lt} = (\mathrm{diag}(\boldsymbol{K}_{droop}^{IV}) + \boldsymbol{G}_{dcm}^{lt})^{-1} \boldsymbol{\mathcal{B}} \\ \boldsymbol{\Delta I}_{dcm}^{IV,lt} = -\mathrm{diag}(\boldsymbol{K}_{droop}^{IV}) \boldsymbol{\Delta V}_{dcm}^{IV,lt} \end{cases} \quad (56)$$

Table 1
Parameters of converters in the MVDC test system.

Parameters	C1	C2	C3	C4	C5	C6	C7	C8
P_{dcr} (MW)	20	20	6	6	7	7	4	3
V_{dcmr} (kV)	20	20	20	20	20	20	20	20
δ_{droop}	0.1	0.1	/	/	/	/	0.1	0.1
K_{droop}	10[a]	0.5[b]	0	0	0	0	2[a]	0.075[b]

[a] P/V droop (MW/kV).
[b] I/V droop (kA/kV).

Table 2
Pre-specified steady-state conditions.

Parameters		T1	T2	T3	T4	T5	T6	T7	T8
P_{dc} (MW)	Case1	/	/	/	/	/	/	2	/
	Case2	/	/	−5	/	/	−6[a]	2	/
V_{dc} (kV)	Case1	20	/	/	/	/	/	/	/
	Case2	20	/	/	/	/	/	/	/
I_{dc} (kA)	Case1	/	0.5	−0.25	−0.25	−0.3	−0.3	/	0.05
	Case2	/	0.5	/	−0.25	−0.3	/	/	0.05

[a] dc power at the LV side of dc/dc converters.

Similar to the dc power/voltage deviation searching process after TS closing in Section 4.1, a proper $\mathcal{K}_{droop,\iota}^{IV,pv}$ can also be found for P/V droop-controlled converter ι if

$$\|\boldsymbol{\Psi}_\iota\|_\infty < \varepsilon_{k,lt}, \text{ and} \quad (57)$$

$\boldsymbol{\Psi}_\iota = [K_{droop,1}^{PV,tar} + \frac{\Delta P_{dcm/l,1}}{\Delta V_{dcm,1}}, \ldots, K_{droop,\rho}^{PV,tar} + \frac{\Delta P_{dcm/l,\iota}}{\Delta V_{dcm,\iota}}]^{-1}$.

Hence, the total dc power, current and voltage deviations in all MV terminals are $\boldsymbol{\Delta I}_{dcm}^{tc} + \boldsymbol{\Delta I}_{dcm}^{co} + \boldsymbol{\Delta I}_{dcm}^{lt}$, $\boldsymbol{\Delta P}_{dcm}^{tc} + \boldsymbol{\Delta P}_{dcm}^{co} + \boldsymbol{\Delta P}_{dcm}^{lt}$ and $\boldsymbol{\Delta V}_{dcm}^{tc} + \boldsymbol{\Delta V}_{dcm}^{co} + \boldsymbol{\Delta V}_{dcm}^{lt}$ respectively, then the final power distribution is acquired under such scenario.

5. Case study

A real-time hybrid AC/MT-MVDC test model (Fig. 11), incorporating an MT-MVDC distribution system with distributed generators and ac/dc loads and modified IEEE 14/33/69 bus systems, is carried out in RSCAD/RTDS to verify the accuracy of the proposed PF algorithm and power distribution analysis method. The MT-MVDC distribution system is expanded from Suzhou industrial park pilot MVDC project [36]. Table 1 lists the parameters of different converters. Converters 1 and 7 (VSCs) adopt P/V droop control, I/V droop control is used in converter 2 (VSC) and converter 8 (dc/dc converter), while other VSCs and dc/dc converters are with constant dc power or dc current control mode. In addition, the reactive power is regulated in VSCs 1, 2 and 4 (0 MVar), the ac voltage control is adopted in VSCs 2, 5 and 6 (147.66 kV for VSC2, 0.4 kV for VSC5, 0.69 kV for VSC6).

5.1. Initial PF of the hybrid AC/MT-MVDC test system

In the initial operation state, the TS in switching station is open and the pre-specified conditions under two cases are shown in Table 2. In case 1, there are one known dc power and 7 known dc currents, while 3 dc power and 4 dc current values are known for case 2. The second case aims to verify the effectiveness of the external searching method when applied to multiple estimated dc current values. The initial PF is implemented using Python with an Intel Core i7-10700 CPU @ 2.90 GHz, 16.0 GB of RAM and a 64-bit Windows 10 operating system.

There are one and three unknown variables (dc currents) in converters 3, 6 and 7 that need to be obtained from the FSNR algorithm under case 1 and case 2, respectively. The dc currents in converters 3, 6 and 7 are first estimated as −0.25 kA, −0.3 kA and 0.1 kA, respectively. With the pre-defined searching ranges ([−0.033, 0.027] kA for converter 3,

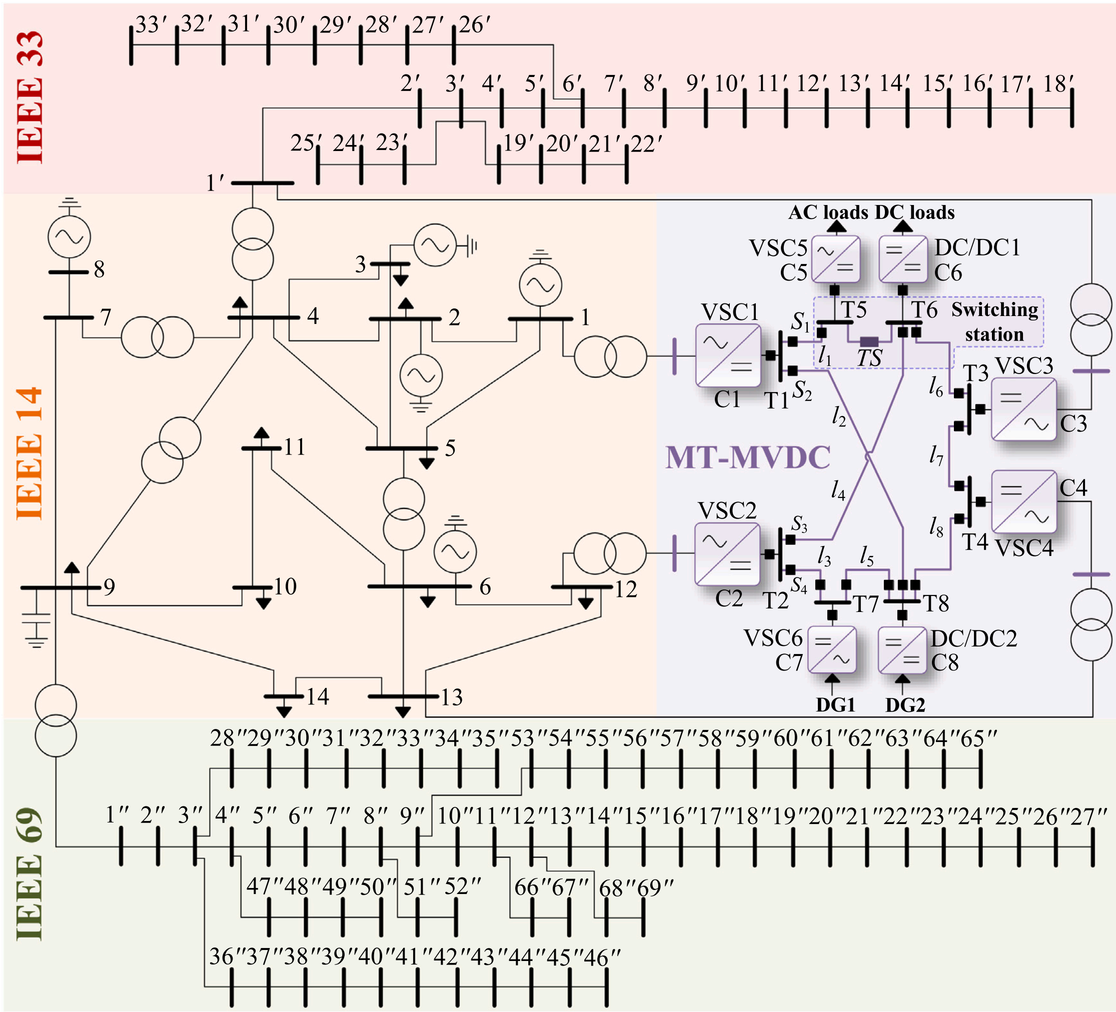

Fig. 11. Hybrid AC/MT-MVDC network incorporating an MT-MVDC distribution system and modified IEEE 14/33/69 bus systems.

[−0.028, 0.023] kA for converter 6, [−0.017, 0.014] kA for converter 7) and iteration targets based on (21) and (23), the accurate dc current values can be found for the two cases. In addition, the dc power at the MVDC bus of converter 6 under case 3 should be calculated based on the known dc power value at the LVDC bus (−6 MW) and equivalent dc/dc converter resistance (set as 0.1 Ω). The A^* shortest path search approach [27] is used to accelerate the searching speed for case 2 with three unknown variables that the dc current in converters 3, 6 and 7 close to the target value is selected to be first corrected.

The conventional decoupled sequential method [15] requires establishing 9 and 25 sub-Jacobian matrices for solving dc PF with the initial steady-state conditions listed in Table 2 under case 1 and case 2, respectively. However, only one Jacobian matrix (18) is constructed in the proposed algorithm, although there are 4 and 8 external correction iterations under case 1 and case 2, respectively. Moreover, the proposed FSNR dc PF algorithm only needs 2 iterations in each external correction iteration since only conductance is included in the Jacobian matrix, while 4 iterations are required in the conventional decoupled sequential method. It should be emphasized that the efficiency of the proposed dc PF algorithm is free from the influence of the future large-scale expansion of MVDC systems, as the quantity of external iterations relies exclusively on the initial dc power values.

In the following HVAC/MVAC PF computation, the HVAC (IEEE 14 bus transmission system) PF is solved after obtaining the total consumed active and reactive power of connected MVDC and MVAC distribution systems. The equivalent impedance for the transformer in VSC station is $R_e = 0.006$ p.u., $X_e = 0.18$ p.u., and $C_1 = 0.003$ p.u., $C_2 = 0.004$ p.u., $C_3 = 0.004$ p.u. for the converter power loss calculation of VSCs. During the MVAC PF derivation process, the BFS method is used and the total power consumptions are $(3.918 + j2.435)$ MVA and $(4.027 + j2.795)$ MVA for IEEE 33 and 69 bus distribution systems, respectively.

In order to demonstrate the validity and efficiency of the proposed PF algorithm in hybrid AC/MT-MVDC system, the conventional sequential coupled and decoupled PF algorithms for HVDC transmission systems are partially modified that dc/dc converters and MVAC distribution networks are further considered. The PF comparison results listed in Table 3 demonstrate the validity of presented sequential PF algorithm. Moreover, the computation efficiency comparison results in Table 4 show the efficiency superiority of presented PF algorithm, whereas external correction iterations in the MVDC PF part could be required if certain dc power values are known to initialize the MVDC PF.

5.2. Power distribution when TS is in NC state under case 2

A very small resistance ($R_{ts,ini} = 10^{-5}$ Ω) between T5 and T6 is assumed for TS, and rank$\left(\mathrm{diag}(\boldsymbol{K}^{IV}_{droop}) + \boldsymbol{G}^{tc}_{dcm}\right) = 8$ showing 10^{-5} Ω is a reasonable value for further calculation. The redistributed power

Table 3
Comparison of PF results.

Converters		P_{dcm} (MW)	I_{dcm} (kA)	V_{dcm} (kV)	P_s (MW)	Q_s (MVar)	V_s (kV)
VSC1 (Case1)	Alg.1	8.99	0.45	20.00	9.14	0	146.28
	Alg.2	8.99	0.45	20.00	9.14	0	146.28
	Presented	8.99	0.45	20.00	9.14	0	146.28
	RSCAD	8.99	0.45	20.00	9.12	0	146.25
VSC1 (Case2)	Alg.1	9.39	0.47	20.00	9.54	0	146.28
	Alg.2	9.39	0.47	20.00	9.54	0	146.28
	Presented	9.39	0.47	20.00	9.54	0	146.28
	RSCAD	9.39	0.47	20.00	9.52	0	146.26
DC/DC1 (Case1)	Alg.1	−5.82	−0.3	19.39	/	/	/
	Alg.2	−5.82	−0.3	19.39	/	/	/
	Presented	−5.82	−0.3	19.39	/	/	/
	RSCAD	−5.82	−0.3	19.39	/	/	/
DC/DC1 (Case2)	Alg.1	−6.01	−0.31	19.34	/	/	/
	Alg.2	−6.01	−0.31	19.34	/	/	/
	Presented	−6.01	−0.31	19.34	/	/	/
	RSCAD	−6.01	−0.31	19.34	/	/	/

Alg.1: Conventional coupled sequential PF algorithm [34]
Alg.2: Conventional decoupled sequential PF algorithm [15].

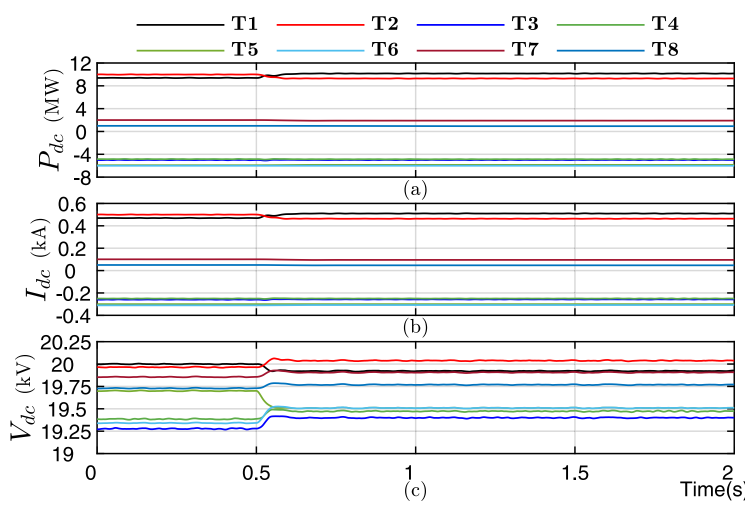

Fig. 12. Waveforms of dc power/current and voltage in all MVDC terminals after closing TS: (a) dc power, (b) dc current and (c) dc voltage.

Table 4
Algorithm efficiency comparison.

Algorithms		Iterations (DC)	Iterations (AC) HV14/MV33/MV69	Time (ms)
Case1	Alg.1	9	13/4/4	1159.1
	Alg.2	4	4/4/4	546.6
	Presented	2 × 4	4/4/4	567.6
Case2	Alg.1	9	13/4/4	1159.1
	Alg.2	4	4/4/4	546.6
	Presented	2 × 8	4/4/4	638.4

distribution when the TS is in NC state can be calculated by (40). Moreover, four dynamic droop coefficients are introduced for P/V droop control-based VSC1, VSC6 and constant dc power control-based VSC3, DC/DC converter 1. The newly obtained droop coefficients (kA/MW) for VSC1, VSC3, DC/DC converter 1 and VSC6 are 0.5255, −0.0134, −0.0159 and 0.1055, respectively with searching range and target value following (42) and (43), respectively.

The real-time simulation results after closing the TS at 0.5 s in switching station are shown in Fig. 12. Moreover, all the calculation and simulation data are listed in Table 5.

5.3. Power distribution after VSC1 or VSC2 outage under case 2

The influence of VSC1 and VSC2 outage to the power distribution is tested that VSC1 (VSC2) is isolated and line1, line2 (line3, line4) are disconnected at 0.5 s after opening S_1 and S_2 (S_3 and S_4). In addition, the TS is closed in order to ensure the load power supply. The calculation results of power/current variations and voltage deviations can be obtained by the proposed three-stage calculation method in Section 4.2. The power distribution in the first calculation stage has been obtained in Section 5.2. In the second calculation stage (VSC1 or VSC2 outage), the droop constant of VSC1 or VSC2 is set as zero and the dc current reference deviations are −0.51 kA and −0.46 kA for VSC1 and VSC2, respectively. The obtained droop coefficients (kA/MW) after VSC1 outage for VSC3, DC/DC1 and VSC6 are −0.0141, −0.0168 and 0.1101, respectively. In addition, the derived droop coefficients (kA/MW) after VSC2 outage for VSC1, VSC3, DC/DC1 and VSC6 are 0.5441, −0.0139, −0.0165, 0.1102, respectively. In the third calculation stage (line disconnection), the corresponding droop coefficients (kA/MW) require to be further modified that −0.0150, −0.0179, 0.1150 are for VSC3, DC/DC1, VSC6 under VSC1 outage, and 0.5622, −0.0145, −0.0173, 0.1147 are for VSC1, VSC3, DC/DC1, VSC6 under VSC1 outage.

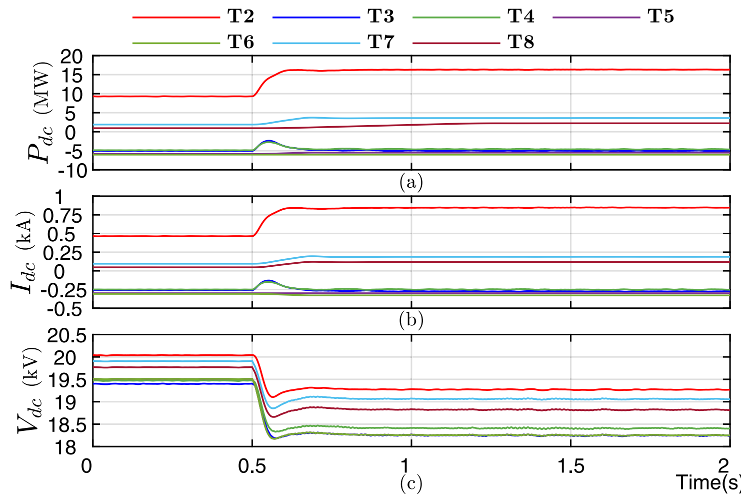

Fig. 13. Waveforms of dc power/current and voltage in all MVDC terminals after VSC1 outage: (a) dc power, (b) dc current and (c) dc voltage.

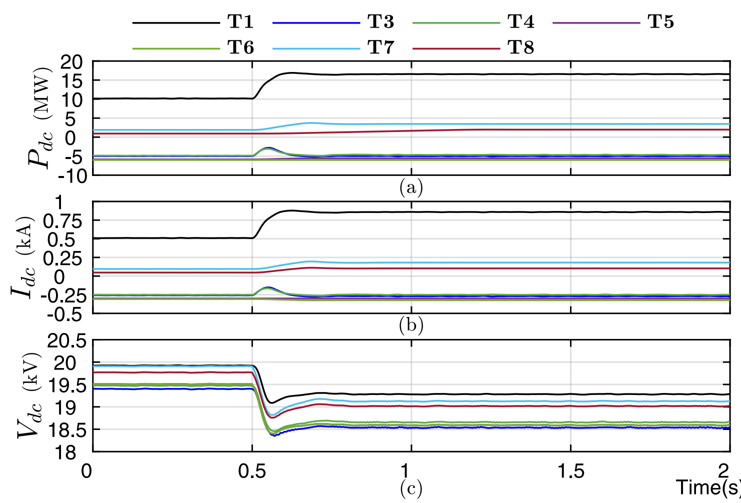

Fig. 14. Waveforms of dc power/current and voltage in all MVDC terminals after VSC2 outage: (a) dc power, (b) dc current and (c) dc voltage.

Table 5
Power distribution after closing TS in switching station.

Terminals		T1	T2	T3	T4	T5	T6	T7	T8
P_{dcm} (MW)	Calculation	10.16	9.29	−5.00	−4.87	−5.85	−6.01	1.90	0.93
	RSCAD	10.16	9.29	−5.00	−4.87	−5.85	−6.01	1.90	0.93
I_{dcm} (MW)	Calculation	0.51	0.46	−0.26	−0.25	−0.30	−0.31	0.10	0.05
	RSCAD	0.51	0.46	−0.26	−0.25	−0.30	−0.31	0.10	0.05
V_{dcm} (kV)	Calculation	19.92	20.04	19.40	19.47	19.51	19.51	19.91	19.77
	RSCAD	19.92	20.04	19.40	19.47	19.51	19.51	19.91	19.77

Figs. 13 and 14 show the waveforms of dc power and voltage in all terminals following VSC1 and VSC2 outage, respectively. Tables 6 and 7 list the corresponding calculation and real-time simulation results.

6. Discussion and conclusion

The proposed sequential PF algorithm has the following advantages: (1) it is suitable for the initial PF determination of hybrid AC/MT-MVDC distribution systems that the HVAC/MVAC PF is computed after the convergence of MVDC PF, and the VSCs and dc/dc converters are considered together in the PF derivation; (2) the MVDC bus type definition is simplified and the solution of multiple Jacobian matrices can be avoided by presented FSNR approach; (3) the definition of single dc current bus type leads to a constant MVDC Jacobian matrix which reduces the number of iterations, although additional external correction iterations are required for dc power buses. (4) the total HVAC PF iterations are fewer than the coupled sequential PF method with several overall HVAC and MVDC PF iterations; Therefore, the proposed PF algorithm offers high availability and reliability in planning and designing future MVDC networks. The PF results from the proposed algorithm, modified conventional algorithms and real-time simulation with RTDS validate the accuracy and efficiency of the

Table 6
Power distribution after VSC1 outage.

Terminals		T2	T3	T4	T5	T6	T7	T8
P_{dcm} (MW)	Calculation	16.32	−5.00	−4.60	−5.48	−6.01	3.59	2.22
	RSCAD	16.32	−5.00	−4.60	−5.48	−6.01	3.59	2.22
I_{dcm} (kA)	Calculation	0.85	−0.27	−0.25	−0.30	−0.33	0.19	0.12
	RSCAD	0.85	−0.27	−0.25	−0.30	−0.33	0.19	0.12
V_{dcm} (kV)	Calculation	19.27	18.25	18.41	18.25	18.25	19.06	18.82
	RSCAD	19.27	18.25	18.41	18.25	18.25	19.06	18.82

Table 7
Power distribution after VSC2 outage.

Terminals		T1	T3	T4	T5	T6	T7	T8
P_{dcm} (MW)	Calculation	16.56	−5.00	−4.66	−5.58	−6.01	3.46	1.97
	RSCAD	16.56	−5.00	−4.66	−5.58	−6.01	3.46	1.97
I_{dcm} (kA)	Calculation	0.86	−0.27	−0.25	−0.30	−0.32	0.18	0.10
	RSCAD	0.86	−0.27	−0.25	−0.30	−0.32	0.18	0.10
V_{dcm} (kV)	Calculation	19.28	18.54	18.66	18.59	18.59	19.13	19.02
	RSCAD	19.28	18.54	18.66	18.59	18.59	19.13	19.02

proposed decoupled sequential PF algorithm for hybrid AC/MT-MVDC systems.

The presented steady-state power distribution analysis method can be used to evaluate the post-event operational security of MT-MVDC systems, by solving the power redistribution in MVDC networks of different closed loop operation modes under coordinated droop control in VSCs and dc/dc converters. For P/V droop-controlled VSCs and dc/dc converters, dynamic I/V droop coefficients are employed for finding the actual dc power, current and voltage deviations according to corresponding P/V droop characteristics. It is worth noting that the power distribution analysis method can achieve zero error calculation as the dc current deviation is linearly related to the dc voltage deviation. The power distribution results from real-time simulation in two closed loop operation modes demonstrate the accuracy of this analysis approach. The proposed method has limitations that future work could address, including the need to incorporate additional constraints for optimizing network losses and minimizing generation costs. However, the proposed hybrid AC/MT-MVDC power flow algorithm, in conjunction with the post-event steady-state power distribution analysis method, already provides accurate and efficient initial power flow determination and precise post-event power redistribution calculations.

CRediT authorship contribution statement

Pingyang Sun: Investigation, Methodology, Validation, Visualization, Writing – original draft, Writing – review & editing. **Rongcheng Wu:** Investigation, Methodology, Validation, Writing – original draft, Writing – review & editing. **Zhiwei Shen:** Investigation, Methodology, Writing – original draft, Writing – review & editing. **Gen Li:** Investigation, Resources, Writing – original draft, Writing – review & editing. **Muhammad Khalid:** Investigation, Resources, Writing – original draft, Writing – review & editing. **Graham Town:** Investigation, Resources, Writing – original draft, Writing – review & editing, Funding acquisition. **Georgios Konstantinou:** Funding acquisition, Investigation, Project administration, Resources, Supervision, Writing – original draft, Writing – review & editing.

Declaration of competing interest

The authors declare that they have no known competing financial interests or personal relationships that could have appeared to influence the work reported in this paper.

Data availability

No data was used for the research described in the article.

Acknowledgments

The authors would like to acknowledge the support provided by Australian Research Council's Discovery Project (DP210102294), and the Deanship of Research Oversight and Coordination and the Interdisciplinary Research Center for Renewable Energy and Power Systems at King Fahd University of Petroleum and Minerals under Project No. INRE2321.

References

[1] CIGRE WG C6/B437. Medium Voltage DC Distribution Systems. CIGRE, Tech. Brochure 875, CIGRE; 2022.
[2] Abeynayake G, et al. Reliability and cost-oriented analysis, comparison and selection of multi-level MVDC converters. IEEE Trans Power Deliv 2021;36(6):3945–55. http://dx.doi.org/10.1109/TPWRD.2021.3051531.
[3] Sun P, Tian Y, Pou J, Konstantinou G. Beyond the MMC: Extended modular multilevel converter topologies and applications. IEEE Open J Power Electron 2022;3:317–33. http://dx.doi.org/10.1109/OJPEL.2022.3175714.
[4] Simiyu P, et al. Review of the DC voltage coordinated control strategies for multi-terminal VSC-MVDC distribution network. The J Eng 2018;2019(16):1462–8. http://dx.doi.org/10.1049/joe.2018.8841.
[5] Ji Y, Yuan Z, Zhao J, Lu C, Wang Y, Zhao Y, et al. Hierarchical control strategy for MVDC distribution network under large disturbance. IET Gener Transm Distrib 2018;12(11):2557–65. http://dx.doi.org/10.1049/iet-gtd.2017.1642.
[6] Simiyu P, Xin A, Wang K, Adwek G, Salman S. Multiterminal medium voltage DC distribution network hierarchical control. Electronics 2020;9(3). http://dx.doi.org/10.3390/electronics9030506.
[7] Petridis S, Blanas O, Rakopoulos D, Stergiopoulos F, Nikolopoulos N, Voutetakis S. An efficient backward/forward sweep algorithm for power flow analysis through a novel tree-like structure for unbalanced distribution networks. Energies 2021;14(4). http://dx.doi.org/10.3390/en14040897.
[8] Karimi M, et al. Application of Newton-based load flow methods for determining steady-state condition of well and ill-conditioned power systems: A review. Int J Elect Power Energy Syst 2019;113:298–309. http://dx.doi.org/10.1016/j.ijepes.2019.05.055.
[9] Montoya OD, Gil-Gonzalez W, Garces A. Optimal power flow on DC microgrids: A quadratic convex approximation. IEEE Trans Circuits Syst II: Exp Briefs 2019;66(6):1018–22. http://dx.doi.org/10.1109/tcsii.2018.2871432.
[10] Huang Y, Ju Y, Ma K, Short M, Chen T, Zhang R, et al. Three-phase optimal power flow for networked microgrids based on semidefinite programming convex relaxation. Appl Energy 2022;305:117771. http://dx.doi.org/10.1016/j.apenergy.2021.117771.
[11] Hamad AA, Azzouz MA, Saadany EFE. A sequential power flow algorithm for islanded hybrid AC/DC microgrids. IEEE Trans Power Syst 2016;31(5):3961–70. http://dx.doi.org/10.1109/tpwrs.2015.2504461.
[12] Aprilia E, Meng K, Al Hosani M, Zeineldin HH, Dong ZY. Unified power flow algorithm for standalone AC/DC hybrid microgrids. IEEE Trans Smart Grid 2019;10(1):639–49. http://dx.doi.org/10.1109/TSG.2017.2749435.
[13] Garces A. On the convergence of Newton's method in power flow studies for DC microgrids. IEEE Trans Power Syst 2018;33(5):5770–7. http://dx.doi.org/10.1109/tpwrs.2018.2820430.

[14] Xia Z, Su M, Liu Z, Zheng M, Zhang X, Wang P. Feasible power-flow solution analysis of DC microgrid considering distributed generations under MPPT control. IEEE Trans Smart Grid 2022;13(1):139–48. http://dx.doi.org/10.1109/tsg.2021.3121773.

[15] Wang W, Barnes M. Power flow algorithms for multi-terminal VSC-HVDC with droop control. IEEE Trans Power Syst 2014;29(4):1721–30. http://dx.doi.org/10.1109/TPWRS.2013.2294198.

[16] Fernández-Pérez J-C, Echavarren Cerezo FM, Rodríguez LR. On the convergence of the sequential power flow for multiterminal VSC AC/DC systems. IEEE Trans Power Syst 2018;33(2):1768–76. http://dx.doi.org/10.1109/TPWRS.2017.2720740.

[17] Gao S, Chen Y, Huang S, Xia Y. Efficient power flow algorithm for AC/MTDC considering complementary constraints of VSC's reactive power and AC node voltage. IEEE Trans Power Syst 2021;36(3):2481–90. http://dx.doi.org/10.1109/TPWRS.2020.3040356.

[18] Chai R, Zhang B, Dou J, Hao Z, Zheng T. Unified power flow algorithm based on the NR method for hybrid AC/DC grids incorporating VSCs. IEEE Trans Power Syst 2016;31(6):4310–8. http://dx.doi.org/10.1109/TPWRS.2015.2511303.

[19] Baradar M, Ghandhari M. A multi-option unified power flow approach for hybrid AC/DC grids incorporating multi-terminal VSC-HVDC. IEEE Trans Power Syst 2013;28(3):2376–83. http://dx.doi.org/10.1109/TPWRS.2012.2236366.

[20] Xiao L, Xu Z, An T, Bian Z. Improved analytical model for the study of steady state performance of droop-controlled VSC-MTDC systems. IEEE Trans Power Syst 2017;32(3):2083–93. http://dx.doi.org/10.1109/TPWRS.2016.2601104.

[21] Sun P, Wickramasinghe HR, Khalid M, Konstantinou G. AC/DC fault handling and expanded DC power flow expression in hybrid multi-converter DC grids. Int J Elect Power Energy Syst 2022;141:107989.

[22] Sun P, Wang Y, Khalid M, Blasco-Gimenez R, Konstantinou G. Steady-state power distribution in VSC-based MTDC systems and DC grids under mixed P/V and I/V droop control. Electr Power Syst Res 2023;214:108798. http://dx.doi.org/10.1016/j.epsr.2022.108798.

[23] Wang Y, et al. Adaptive voltage droop method of multiterminal VSC-HVDC systems for DC voltage deviation and power sharing. IEEE Trans Power Deliv 2019;34(1):169–76. http://dx.doi.org/10.1109/TPWRD.2018.2844330.

[24] Zhang Y, Wang L, Li W. Autonomous DC line power flow regulation using adaptive droop control in HVDC grid. IEEE Trans Power Deliv 2021;36(6):3550–60. http://dx.doi.org/10.1109/TPWRD.2020.3044978.

[25] Haileselassie TM, Uhlen K. Impact of DC line voltage drops on power flow of MTDC using droop control. IEEE Trans Power Syst 2012;27(3):1441–9. http://dx.doi.org/10.1109/TPWRS.2012.2186988.

[26] Subasi M, Yildirim N, Yildiz B. An improvement on Fibonacci search method in optimization theory. Appl Math Comput 2004;147(3):893–901. http://dx.doi.org/10.1016/S0096-3003(02)00828-7.

[27] Candra A, Budiman MA, Hartanto K. Dijkstra's and A-star in finding the shortest path: A tutorial. In: 2020 int. conf. on data sci., artificial intell., and bus. analytics. 2020, p. 28–32. http://dx.doi.org/10.1109/DATABIA50434.2020.9190342.

[28] Li B, Yu X, Bo Z. Protection schemes for closed loop distribution network with distributed generator. In: 2009 int. conf. sustainable power generation and supply. 2009, p. 1–6. http://dx.doi.org/10.1109/SUPERGEN.2009.5348370.

[29] Kong T, Cheng H, Hu Z, Yao L. Multiobjective planning of open-loop MV distribution networks using ComGIS network analysis and MOGA. Electr Power Syst Res 2009;79(2):390–8.

[30] Zhao Y, Xiong W, Yuan X, Zou X. A fault recovery strategy of flexible interconnected distribution network with SOP flexible closed-loop operation. Int J Elect Power Energy Syst 2022;142:108360.

[31] Liu D, Zhang C, Chen G, Xu Y, Dong ZY. Stochastic security-constrained optimal power flow for a microgrid considering tie-line switching. Int J Elect Power Energy Syst 2022;134:107357.

[32] Sebaa K, Kahouli O. DC transformer for optimal power flow with interior point algorithm. In: 2018 15th int. multi-conf. on syst., signals & devices. 2018, p. 543–7. http://dx.doi.org/10.1109/SSD.2018.8570368.

[33] Javid Z, Karaagac U, Kocar I, Xue T. DC grid load flow solution incorporating generic DC/DC converter topologies. Energy Rep 2023;9:951–61. http://dx.doi.org/10.1016/j.egyr.2023.05.164, 2022 The 3rd International Conference on Power and Electrical Engineering.

[34] Beerten J, Cole S, Belmans R. Generalized steady-state VSC MTDC model for sequential AC/DC power flow algorithms. IEEE Trans Power Syst 2012;27(2):821–9. http://dx.doi.org/10.1109/TPWRS.2011.2177867.

[35] Zhao B, Song Q, Li J, Sun Q, Liu W. Full-process operation, control, and experiments of modular high-frequency-link DC transformer based on dual active bridge for flexible MVDC distribution: A practical tutorial. IEEE Trans Power Electron 2017;32(9):6751–66. http://dx.doi.org/10.1109/TPEL.2016.2626262.

[36] Fan Y, Chi Y, Li Y, Wang Z, Liu H, Liu W, et al. Key technologies for medium and low voltage DC distribution system. Global Energy Interconnect 2021;4(1):91–103. http://dx.doi.org/10.1016/j.gloei.2021.03.009.